Journal of Computational Physics 396 (2019) 228–242

Contents lists available at ScienceDirect

Journal of Computational Physics

www.elsevier.com/locate/jcp

Edge multiscale methods for elliptic problems with heterogeneous coefficients

Shubin Fu [a], Eric Chung [a,1], Guanglian Li [b,*,2]

[a] Department of Mathematics, The Chinese University of Hong Kong, Hong Kong Special Administrative Region
[b] Department of Mathematics, Imperial College London, South Kensington, London SW7 2AZ, UK

ARTICLE INFO

Article history:
Received 24 October 2018
Received in revised form 4 June 2019
Accepted 5 June 2019
Available online 27 June 2019

Keywords:
Multiscale
Heterogeneous
Edge
High-contrast
Steklov eigenvalue
Wavelets

ABSTRACT

In this paper, we proposed two new types of edge multiscale methods motivated by [14] to solve Partial Differential Equations (PDEs) with high-contrast heterogeneous coefficients: Edge Spectral Multiscale Finite Element Method (ESMsFEM) and Wavelet-based Edge Multiscale Finite Element Method (WEMsFEM). Their convergence rates for elliptic problems with high-contrast heterogeneous coefficients are demonstrated in terms of the coarse mesh size H, the number of spectral basis functions and the level of the wavelet space ℓ, which are verified by extensive numerical tests.

1. Introduction

The accurate mathematical modeling of many important applications, e.g., composite materials, porous media and reservoir simulation, involves elliptic problems with heterogeneous coefficients. In order to adequately describe the intrinsic complex properties in practical scenarios, the heterogeneous coefficients can have both multiple inseparable scales and high-contrast. Due to this disparity of scales, the classical numerical treatment becomes prohibitively expensive and even intractable for many multiscale applications. Nonetheless, motivated by the broad spectrum of practical applications, a large number of multiscale model reduction techniques, e.g., multiscale finite element methods (MsFEMs), heterogeneous multiscale methods (HMMs), variational multiscale methods, flux norm approach, generalized multiscale finite element methods (GMsFEMs) and localized orthogonal decomposition (LOD), have been proposed in the literature [11,5,12,2,6,17,15] over the last few decades. They have achieved great success in the efficient and accurate simulation of heterogeneous problems. Amongst these numerical methods, the GMsFEMs [6] have demonstrated extremely promising numerical results for a wide variety of problems, and thus they are becoming increasingly popular.

However, the mathematical understanding of GMsFEMs remains largely missing, despite numerous successful empirical evidences. Recently, the author in [14] provided a first mathematical justification without any restrictive assumptions or

* Corresponding author.
E-mail addresses: shubinfu89@gmail.com (S. Fu), eric.t.chung@gmail.com (E. Chung), lotusli0707@gmail.com, guanglian.li@imperial.ac.uk (G. Li).

[1] EC is partially supported by Hong Kong RGC General Research Fund (Project 14304217) and CUHK Direct Grant for Research 2017-18.
[2] GL acknowledges the support from the Royal Society through a Newton international fellowship (NF170124). Part of this work was done while EC and GL visited Erwin Schrödinger International Institute for Mathematics and Physics (ESI, Vienna) for the research program: Numerical Analysis of Complex PDE Models in the Sciences.

https://doi.org/10.1016/j.jcp.2019.06.006
0021-9991/

oversampling technique by representing the solution restricted on each local domain as a summation of three parts, and then approximating rigorously each component by means of precalculated multiscale basis functions, namely, a specific multiscale basis function, local multiscale basis functions over the local domain and over the coarse edges. One of the critical challenges in [14] is to make every estimate independent of the heterogeneity in the coefficient, e.g., the multiple scales and large deviation of values. As proved in [14], among the three types of multiscale basis functions to approximate each component of the solution over each local region, the local multiscale basis functions over the coarse edges play a critical role. Its energy error estimate poses a certain difficulty in the proof, which relies mainly on the regularity properties [3,13] of the high-contrast problems and the transposition method [16]. In particular, the approximation property of the solution over the coarse edges determines the approximation of the solution in energy norm.

Motivated by this result, we propose two types of Edge Multiscale Finite Element Methods in Section 4 to solve PDEs with heterogeneous coefficients: Edge Spectral Multiscale Finite Element Method (ESMsFEM) and Wavelet-based Edge Multiscale Finite Element Method (WEMsFEM). The edge spectral multiscale basis functions and the wavelets (e.g., Haar wavelets and hierarchical bases) [4,20] are utilized to approximate the trace of the solution over each coarse edge, correspondingly. On the one hand, due to the large variations and discontinuities in the heterogeneous coefficients, this gives arise to singular behavior and the solution owns very low regularity in certain regions of the computational domain. On the other hand, the wavelets are capable of approximating functions with very low regularities and their approximation properties are reflected or characterized by the size of the finest level. Moreover, the hierarchical structure intrinsically built in the wavelets makes the wavelets excellent candidates to approximate functions with low regularities. For this reason, we apply the wavelets as the basis functions on the edges. In addition, we derive the energy error estimates for each approach and present several numerical tests in 2-dimension and 3-dimension to demonstrate the accuracy of our new proposed methods. We noticed that there is another type of Edge Multiscale Finite Element Method proposed in [10] utilizing the eigenfunctions of some oversampling operator to obtain the basis functions over the coarse edges, which is different from our approach.

This work is not the first one to apply ideas from wavelets to approximating multiscale partial differential equations. The authors in [8] proposed a projection-based numerical homogenization scheme which utilizes different levels of wavelet spaces as the coarse space and the fine space. In specific, this procedure involves global correction operators over the computational domain, and the wavelets are utilized to approximate the solution directly. Recently, wavelets are applied to derive an orthogonal decomposition of the solution [19], which again, approximate the solution on the global or localized domain directly. To the best of our knowledge, this paper represents the first one, where the wavelets are introduced to approximate the trace of the solution over each coarse edge. Because of this, there is no further localization technique required in our methods.

The remainder of the paper is arranged as below. We formulate in Section 2 the heterogeneous elliptic problem and the main idea of GMsFEMs. Then we present the basic notation and approximation properties of Haar wavelets and hierarchical bases in Section 3. This is then followed by Section 4 dealing with two novel edge multiscale methods, which are the key findings of this paper. Their theoretical and numerical performance are presented in Sections 5 and 6. Finally, we conclude the paper with several remarks in Section 7.

2. Preliminaries

We first formulate the heterogeneous elliptic problem to present our new multiscale methods. Let $D \subset \mathbb{R}^d$ $(d = 1, 2, 3)$ be an open bounded Lipschitz domain with a boundary ∂D. We seek a function $u \in V := H_0^1(D)$ such that

$$\begin{aligned} \mathcal{L}u := -\nabla \cdot (\kappa \nabla u) &= f \qquad \text{in } D, \\ u &= 0 \qquad \text{on } \partial D, \end{aligned} \tag{2.1}$$

where the force term $f \in L^2(D)$ and the permeability coefficient $\kappa \in L^\infty(D)$ with $\alpha \le \kappa(x) \le \beta$ almost everywhere for some lower bound $\alpha > 0$ and upper bound $\beta > \alpha$. We denote by $\Lambda := \frac{\beta}{\alpha}$ the ratio of these bounds, which reflects the contrast of the coefficient κ. Note that the existence of multiple scales in the coefficient κ rends directly solving Problem (2.1) challenging, since resolving the problem to the finest scale would incur huge computational cost.

Now we present basic facts related to Problem (2.1) and briefly describe the GMsFEM (and also to fix the notation). Let the space $V := H_0^1(D)$ be equipped with the (weighted) inner product

$$\langle v_1, v_2 \rangle_D =: a(v_1, v_2) := \int_D \kappa \nabla v_1 \cdot \nabla v_2 \, \mathrm{d}x \quad \text{for all } v_1, v_2 \in V,$$

and the associated energy norm

$$|v|^2_{H^1_\kappa(D)} := \langle v, v \rangle_D \quad \text{for all } v \in V.$$

We denote by $(\cdot, \cdot)_D$ as the inner product in $L^2(D)$.

The weak formulation for problem (2.1) is to find $u \in V$ such that

$$a(u, v) = (f, v)_D \quad \text{for all } v \in V. \tag{2.2}$$

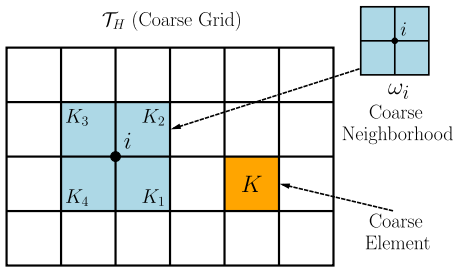

Fig. 1. Illustration of a coarse neighborhood and coarse element.

The Lax-Milgram theorem implies the well-posedness of problem (2.2).

To discretize problem (2.1), we first introduce fine and coarse grids. Let $\mathcal{T}_H$ be a regular partition of the domain D into finite elements (triangles, quadrilaterals, tetrahedral, etc.) with a mesh size H. We refer to this partition as coarse grids, and its elements as the coarse elements. Then each coarse element is further partitioned into a union of connected fine grid blocks. The fine-grid partition is denoted by $\mathcal{T}_h$ with h being its mesh size. Let $\mathcal{F}_h$ (or $\mathcal{F}_H$) be the collection of all edges in $\mathcal{T}_h$ (or $\mathcal{T}_H$), and let $\mathcal{F}_h(\partial\omega_i)$ (or $\mathcal{F}_H(\partial\omega_i)$) be the restriction of $\mathcal{F}_h$ on $\partial\omega_i$ (or $\mathcal{F}_H$ on $\partial\omega_i$). Over the fine mesh $\mathcal{T}_h$, let V_h be the conforming piecewise linear finite element space:

$$V_h := \{v \in V : V|_T \in \mathcal{P}_1(T) \text{ for all } T \in \mathcal{T}_h\},$$

where $\mathcal{P}_1(T)$ denotes the space of linear polynomials on the fine element $T \in \mathcal{T}_h$. Then the fine-scale solution $u_h \in V_h$ satisfies

$$a(u_h, v_h) = (f, v_h)_D \quad \text{for all } v_h \in V_h. \tag{2.3}$$

The fine-scale solution u_h will serve as a reference solution in Section 6. Note that due to the presence of multiple scales in the coefficient κ, the fine-scale mesh size h should be commensurate with the smallest scale and thus it can be very small in order to obtain an accurate solution. This necessarily involves huge computational complexity, and more efficient methods are in great demand.

In this work, we are concerned with flow problems with high-contrast heterogeneous coefficients, which involve multiscale permeability fields, e.g., permeability fields with vugs and faults, and furthermore, can be parameter-dependent, e.g., viscosity. Under such scenario, the computation of the fine-scale solution u_h is vulnerable to high computational complexity, and one has to resort to multiscale methods. The GMsFEM has been extremely successful for solving multiscale flow problems, which we briefly recap below.

The GMsFEM aims at solving Problem (2.1) on the coarse mesh $\mathcal{T}_H$ cheaply, which, meanwhile, maintains a certain accuracy compared to the fine-scale solution u_h. To describe the GMsFEM, we need a few notations. The vertices of $\mathcal{T}_H$ are denoted by $\{O_i\}_{i=1}^N$, with N being the total number of coarse nodes. The coarse neighborhood associated with the node O_i is denoted by

$$\omega_i := \bigcup \{K_j \in \mathcal{T}_H : \quad O_i \in \overline{K}_j\}. \tag{2.4}$$

We refer to Fig. 1 for an illustration of neighborhoods and elements subordinated to the coarse discretization $\mathcal{T}_H$. Throughout, we use ω_i to denote a coarse neighborhood.

Next, we outline the GMsFEM with a conforming Galerkin (CG) formulation. Let $1 \le i \le N$ be a certain coarse node. Note that ω_i is the support of the multiscale basis functions to be identified, and $\ell_i \in \mathbb{N}_+$ is the number of those multiscale basis functions associated with ω_i. They are denoted as $\psi_k^{\omega_i}$ for $k = 1, \cdots, \ell_i$. Throughout, the subscript i denotes the i-th coarse node or coarse neighborhood. Generally, the GMsFEM utilizes multiple basis functions per coarse neighborhood ω_i, and the index k represents the numbering of these basis functions. In turn, the CG multiscale solution u_{ms} is sought as $u_{\text{ms}} = \sum_{i=1}^{N} \sum_{k=1}^{\ell_i} c_k^i \psi_k^{\omega_i}$. Once the basis functions $\psi_k^{\omega_i}$ are identified, the CG global coupling is given through the variational form

$$a(u_{\text{ms}}, v) = (f, v)_D, \quad \text{for all } v \in V_{\text{ms}}, \tag{2.5}$$

where V_{ms} denotes the multiscale space spanned by these multiscale basis functions.

We conclude the section with the following assumption on the computational domain D and the heterogeneous coefficient κ.

Assumption 2.1 *(Structure of D and κ).* Let D be a domain with a $C^{1,\alpha}$ $(0<\alpha<1)$ boundary ∂D, and $\{D_i\}_{i=1}^m \subset D$ be m pairwise disjoint strictly convex open subsets, each with a $C^{1,\alpha}$ boundary $\Gamma_i := \partial D_i$, and denote $D_0 = D\backslash\overline{\cup_{i=1}^m D_i}$. Let the permeability coefficient κ be piecewise regular function defined by

$$\kappa = \begin{cases} \eta_i(x) & \text{in } D_i, \\ 1 & \text{in } D_0. \end{cases} \tag{2.6}$$

Here $\eta_i \in C^{\mu}(\bar{D}_i)$ with $\mu \in (0,1)$ for $i = 1, \cdots, m$. Denote $\eta_{\min} := \min_i\{\min_{x\in D_i}\{\eta_i(x)\}\} \geq 1$ and $\eta_{\max} := \max_i\{\|\eta_i\|_{C_0(D_i)}\}$.

3. Hierarchical subspace splitting over $I =: [0,1]$

In this section, we introduce two types of wavelets on the unit interval $I := [0,1]$: Haar wavelets and hierarchical bases. They facilitate hierarchically splitting the space $L^2(I)$.

3.1. Haar wavelets

Let the level parameter and the mesh size be ℓ and $h_\ell := 2^{-\ell}$ with $\ell \in \mathbb{N}$, respectively. Then the grid points on level ℓ are

$$x_{\ell,j} = j \times h_\ell, \qquad 0 \leq j \leq 2^\ell.$$

Let the scaling function $\phi(x)$ and the mother wavelet $\psi(x)$ be given by

$$\phi(x) = \begin{cases} 1, & \text{if } 0 \leq x \leq 1, \\ 0, & \text{otherwise,} \end{cases} \qquad \psi(x) = \begin{cases} 1, & \text{if } 0 \leq x \leq 1/2, \\ -1, & \text{if } 1/2 < x \leq 1, \\ 0, & \text{otherwise.} \end{cases}$$

By means of dilation and translation, the mother wavelet $\psi(x)$ can result in orthogonal decomposition of the space $L^2(I)$. To this end, we can define the basis functions on level ℓ by

$$\psi^{\mathrm{I}}_{\ell,j}(x) := 2^{\frac{\ell-1}{2}}\psi(2^{\ell-1}x - j) \quad \text{for all} \quad 0 \leq j \leq 2^{\ell-1} - 1.$$

The subspace of level ℓ is

$$W^{\mathrm{I}}_\ell := \begin{cases} \mathrm{span}\{\phi\} & \text{for } \ell = 0 \\ \mathrm{span}\{\psi^{\mathrm{I}}_{\ell,j}: \quad 0 \leq j \leq 2^{\ell-1} - 1\} & \text{for } \ell \geq 1. \end{cases}$$

Note that the subspace W^{I}_ℓ is orthogonal to $W^{\mathrm{I}}_{\ell'}$ in $L^2(I)$ for any two different levels $\ell \neq \ell'$. We denote by V^{I}_ℓ as the subspace in $L^2(I)$ up to level ℓ, which is defined by

$$V^{\mathrm{I}}_\ell := \oplus_{m\leq\ell} W^{\mathrm{I}}_m.$$

Due to the orthogonality of the subspaces W_ℓ on different levels, there holds

$$V^{\mathrm{I}}_{\ell+1} = V^{\mathrm{I}}_\ell \oplus_{L^2(I)} W^{\mathrm{I}}_{\ell+1}.$$

Consequently, it yields the hierarchical structure of the subspace V_ℓ, namely,

$$V^{\mathrm{I}}_0 \subset V^{\mathrm{I}}_1 \subset \cdots \subset V^{\mathrm{I}}_\ell \subset V^{\mathrm{I}}_{\ell+1} \cdots$$

Furthermore, the following orthogonal decomposition of the space $L^2(I)$ holds

$$L^2(I) = \oplus_\ell W^{\mathrm{I}}_\ell.$$

3.2. Hierarchical bases

Let the level parameter and the mesh size be ℓ and $h_\ell := 2^{-\ell}$ with $\ell \in \mathbb{N}$, respectively. Then the grid points on level ℓ are

$$x_{\ell,j} = j \times h_\ell, \qquad 0 \leq j \leq 2^\ell.$$

We can define the basis functions on level ℓ by

$$\psi^{\mathrm{II}}_{\ell,j}(x) = \begin{cases} 1 - |x/h_\ell - j|, & \text{if } x \in [(j-1)h_\ell, (j+1)h_\ell] \cap [0,1], \\ 0, & \text{otherwise.} \end{cases}$$

Define the set on each level ℓ by

$$B_\ell := \left\{ j \in \mathbb{N} \,\middle|\, \begin{array}{ll} j = 1, \cdots, 2^\ell - 1, \, j \text{ is odd}, & \text{if } \ell > 0 \\ j = 0, 1, & \text{if } \ell = 0 \end{array} \right\}.$$

The subspace of level ℓ is

$$W_\ell^{\mathrm{II}} := \operatorname{span}\{\psi_{\ell,j}^{\mathrm{II}} : \quad j \in B_\ell\}.$$

We denote V_ℓ as the subspace in $L^2(I)$ up to level ℓ, which is defined by the direct sum of subspaces

$$V_\ell^{\mathrm{II}} := \oplus_{m \le \ell} W_m^{\mathrm{II}}.$$

Consequently, this yields the hierarchical structure of the subspace V_ℓ, namely,

$$V_0^{\mathrm{II}} \subset V_1^{\mathrm{II}} \subset \cdots \subset V_\ell^{\mathrm{II}} \subset V_{\ell+1}^{\mathrm{II}} \cdots$$

Furthermore, the following hierarchical decomposition of the space $L^2(I)$ holds

$$L^2(I) = \lim_{\ell \to \infty} \oplus_{m \le \ell} W_m^{\mathrm{II}}.$$

Note that one can derive the hierarchical decomposition of the space $L^2(I^d)$ for $d > 1$ by means of tensor product. Note further that we will use the subspace V_ℓ^{I} and V_ℓ^{II} to approximate the restriction of the exact solution u on each coarse edge.

In this paper, we will only focus on the convergence analysis of multiscale algorithms, cf. Algorithm 2, based upon the Haar wavelets V_ℓ^{I}. The convergence analysis of multiscale algorithms based upon the hierarchical bases V_ℓ^{II} can be derived similarly.

Throughout this paper, $(\cdot,\cdot)_T$ denotes the inner product in the Hilbert space $L^2(T)$ for some domain $T \subset D$ or some edges $T \subset \partial\omega_i$. We use $A \lesssim B$ if $A \le CB$ for some benign constant that is independent of the multiple scales and high contrast in the coefficient κ and the coarse scale mesh size H.

Proposition 3.1 *(Approximation properties of the hierarchical space V_ℓ^{I}). Let P_ℓ be $L^2(I)$-orthogonal projection onto V_ℓ^{I} for each level $\ell \ge 0$ and let $s > 0$. Then there holds*

$$P_{\ell+1} v = P_\ell v + \sum_{j=0}^{2^\ell - 1} (v, \psi_{\ell+1,j}^{\mathrm{I}})_I \psi_{\ell+1,j}^{\mathrm{I}} \qquad \text{for all } v \in L^2(I)$$

$$\|v - P_\ell v\|_{L^2(I)} \lesssim 2^{-s\ell} |v|_{H^s(I)} \qquad \text{for all } v \in H^s(I).$$

Proof. The first assertion can be found in [4]. To prove the second assertion, define the operator

$$\mathcal{T} : H^s(I) \to L^2(I) \quad \text{by } \mathcal{T} v := v - P_\ell v.$$

Let $s := 0$. Then the $L^2(I)$-orthogonality of P_ℓ implies

$$\|\mathcal{T} v\|_{L^2(I)} := \|v - P_\ell v\|_{L^2(I)} \le \|v\|_{L^2(I)} \quad \text{for all } v \in L^2(I).$$

Furthermore, let $s := 1$. Since the residual $v - P_\ell v$ is orthogonal to V_ℓ^{I}. Therefore, we obtain

$$\int_{j \times 2^{-\ell}}^{(j+1) \times 2^{-\ell}} (v - P_\ell v) \, \mathrm{d}x = 0 \text{ for all } j = 0, \cdots 2^\ell - 1.$$

Consequently, for all $v \in H^1(I)$, the Poincaré inequality leads to

$$\begin{aligned} \|\mathcal{T} v\|_{L^2(I)}^2 := \|v - P_\ell v\|_{L^2(I)}^2 &= \sum_{j=0}^{2^\ell - 1} \int_{j \times 2^{-\ell}}^{(j+1) \times 2^{-\ell}} |v - P_\ell v|^2 \, \mathrm{d}x \\ &\lesssim 2^{-2\ell} |v|_{H^1(I)}^2. \end{aligned}$$

Taking the square root on both sides gives

$$\|\mathcal{T} v\|_{L^2(I)} \lesssim 2^{-\ell} |v|_{H^1(I)} \quad \text{for all } v \in H^1(I).$$

Finally, the preceding two estimates, together with the interpolation theory, prove the second assertion. □

4. Edge multiscale methods

We propose in this section two new multiscale methods based on GMsFEMs. In specific, their multiscale basis functions are defined locally on each coarse neighborhood independently, and thereby they can be calculated in parallel. The first multiscale method utilizes the dominant eigenvectors from the local Stechlov eigenvalue problem as the local multiscale basis functions. The second one uses wavelets to approximate the solution restricted on each coarse edge. To obtain conforming global basis functions, we utilize the Partition of Unity finite element method [18,7]. Its main idea is to seek local multiscale basis functions in each coarse neighborhood which own certain approximation properties to the exact solution restricted on each coarse neighborhood, and to use the fact that the global multiscale basis functions obtained from those local multiscale basis functions by the partition of unity functions inherit these approximation properties.

To this end, we begin with an initial coarse space $V_0^{\text{init}} = \text{span}\{\chi_i\}_{i=1}^N$. The functions χ_i are the standard multiscale basis functions on each coarse element $K \in \mathcal{T}_H$ defined by

$$\begin{aligned} -\nabla\cdot(\kappa(x)\nabla\chi_i) &= 0 \qquad \text{in } K, \\ \chi_i &= g_i \qquad \text{on } \partial K, \end{aligned} \tag{4.1}$$

where g_i is affine over ∂K with $g_i(O_j) = \delta_{ij}$ for all $i, j = 1, \cdots, N$. Recall that $\{O_j\}_{j=1}^N$ are the set of coarse nodes on $\mathcal{T}_H$. Next we define the weighted coefficient:

$$\widetilde{\kappa} = H^2\kappa\sum_{i=1}^{N}|\nabla\chi_i|^2. \tag{4.2}$$

Furthermore, let $\widetilde{\kappa}^{-1}$ be defined by

$$\widetilde{\kappa}^{-1}(x) = \begin{cases} \widetilde{\kappa}^{-1}, & \text{when } \widetilde{\kappa}(x) \neq 0 \\ 1, & \text{otherwise}. \end{cases} \tag{4.3}$$

The weighted $L^2(D)$ space is

$$L^2_{\widetilde{\kappa}^{-1}}(D) := \left\{ w : \|w\|^2_{L^2_{\widetilde{\kappa}^{-1}}(D)} := \int_D \widetilde{\kappa}^{-1} w^2 \,\mathrm{d}x < \infty \right\}.$$

Note that there are many other alternatives for the partition of unity functions besides using the multiscale basis functions (4.1), e.g., one can utilize the flat top type of partition of unity functions proposed in [9].

4.1. Edge Spectral Multiscale Finite Element Method

The first new multiscale method, coined as the edge spectral multiscale method (ESMsFEM), is inspired by the recent results derived in [14]. To obtain a good approximation space for the solution u in (2.1), one only needs to derive a good local approximation space on each coarse neighborhood ω_i to $u|_{\omega_i}$ according to the main theory of Partition of Unity Finite Element Method [18]. In that paper, the restriction $u|_{\omega_i}$ is split into three components, each of which is approximated by local multiscale basis functions with proved convergence rate. Since one of the components is of $\mathcal{O}(H)$, this part is negligible and is removed from Algorithm 1.

Algorithm 1 Edge Spectral Multiscale Finite Element Method (ESMsFEM).

Input:	Coarse neighborhood ω_i and its total number N; the number of multiscale basis functions $\ell_i \in \mathbb{N}_+$; the partition of unity function χ_i;
Output:	Multiscale solution $u_{\text{ms}}^{\text{ES}}$.
1.	Solve for the Steklov eigenvalue problem and reorder the eigenvalues non-decreasingly. Seek $(\lambda_j^{\text{T}_i}, v_j^{\text{T}_i}) \in \mathbb{R} \times H^1_\kappa(\omega_i)$ such that $\begin{cases} -\nabla\cdot(\kappa\nabla v_j^{\text{T}_i}) = 0 & \text{in } \omega_i, \\ \kappa\frac{\partial}{\partial n} v_j^{\text{T}_i} = \lambda_j^{\text{T}_i}\widetilde{\kappa} v_j^{\text{T}_i} & \text{on } \partial\omega_i. \end{cases}$
2.	Solve one local problem. $\begin{cases} -\nabla\cdot(\kappa\nabla v^i) = \dfrac{\widetilde{\kappa}}{\int_{\omega_i}\widetilde{\kappa}\,\mathrm{d}x} & \text{in } \omega_i, \\ -\kappa\dfrac{\partial v^i}{\partial n} = \lvert\partial\omega_i\rvert^{-1} & \text{on } \partial\omega_i. \end{cases}$
3.	Build global multiscale space. $V_{\text{ms}}^{\text{ES}} := \text{span}\{\chi_i v^i, \chi_i v_k^{\text{T}_i} : \ 1 \le i \le N, \ \ 1 \le k \le \ell_i - 1\}$.
4.	Solve for (2.5) by conforming Galerkin method in $V_{\text{ms}}^{\text{ES}}$ to obtain $u_{\text{ms}}^{\text{ES}}$.

Algorithm 1 proceeds as follows. Recall that N denotes the total number of coarse nodes in the coarse mesh $\mathcal{T}_H$ and ω_i is the coarse neighborhood for the ith coarse node. χ_i is the partition of unity function defined on ω_i, cf. (4.1). Let $1 < \ell_i \in \mathbb{N}_+$ be the number of local multiscale basis functions on this coarse neighborhood ω_i. Among them, the first $\ell_i - 1$ are the dominant modes from the local Steklov eigenvalue problem, cf. Step 1. The last one arises from one specific local solver defined in Step 2. In Step 3, the global multiscale space $V_{\text{ms}}^{\text{ES}}$ is defined with the help of the partition of unity functions $\{\chi_i\}_{i=1}^N$. Then the multiscale solution $u_{\text{ms}}^{\text{ES}}$ is obtained by solving (2.5) in the global multiscale space $V_{\text{ms}}^{\text{ES}}$.

4.2. Wavelet-based Edge Multiscale Finite Element Method

Motivated by [14], the local multiscale basis functions restricted on $\partial\omega_i$, which can approximate $u|_{\partial\omega_i}$ plays a vital role in approximating the solution $u \in V$ in (2.1) efficiently. In view that $u|_{\partial\omega_i} \in H^s(\partial\omega_i)$ for some positive constant $s \geq 1/2$ and the approximation properties of the Haar wavelets, cf. Proposition 3.1, the κ-harmonic functions with the Haar wavelets as the local boundary conditions lend themselves to excellent candidates for the local multiscale basis functions. Combining with the Partition of Unity Finite Element Methods and the conforming Galerkin approximation, this results in a new multiscale method, which is named as the Wavelet-based Edge Multiscale Finite Element Method (WEMsFEM), cf. Algorithm 2.

Remark 4.1 *(Local solvers in Algorithm 2).* The boundary conditions in Step 2 are imposed weakly and the global multiscale basis functions belongs to $H^1(D)$. Recall that $\mathcal{T}_h$ is the fine scale partition of the computational domain D with mesh size $h \ll H$, $\mathcal{F}_h$ is the collection of all edges in $\mathcal{T}_h$ and $\mathcal{F}_h(\partial\omega_i)$ denotes the restriction of $\mathcal{F}_h$ on $\partial\omega_i$. The finite element space over $\partial\omega_i$ is

$$V_h(\partial\omega_i) = \{v \in H^{1/2}(\partial\omega_i) : V|_E \in \mathcal{P}_1(E) \text{ for all } E \in \mathcal{F}_h(\partial\omega_i)\}.$$

In practice, one can solve for an approximation of v, namely, $v_h \in H^1(\omega_i)$, s.t.,

$$\begin{cases} \mathcal{L}_i v_h := -\nabla\cdot(\kappa\nabla v_h) = 0 & \text{in } \omega_i, \\ v_h = I_h^{\partial,i}(v_k) & \text{on } \partial\omega_i. \end{cases}$$

Here, $I_h^{\partial,i}$ denotes the $L^2(\partial\omega_i)$-projection onto $V_h(\partial\omega_i)$. Note that

$$\|v - v_h\|_{L^2(\partial\omega_i)} \lesssim 2^{-\ell/2}\Big(\frac{h}{H}\Big)^{1/2}\|v\|_{L^2(\partial\omega_i)}.$$

Since we are interested in a multiscale algorithm with energy error of $\mathcal{O}(H)$ and since $h \ll H$, the error between v and v_h can be ignored.

Algorithm 2 Wavelet-based Edge Multiscale Finite Element Method (WEMsFEM).

Input:	The level parameter $\ell \in \mathbb{N}$; coarse neighborhood ω_i and its four coarse edges $\Gamma_{i,k}$ with $k = 1, 2, 3, 4$, i.e., $\cup_{k=1}^4 \Gamma_{i,k} = \partial\omega_i$; the subspace $V_{\ell,k}^i \subset L^2(\Gamma_{i,k})$ up to level ℓ on each coarse edge $\Gamma_{i,k}$;
Output:	Multiscale solution $u_{\text{ms},\ell}^{\text{EW}}$.
1.	Denote $V_{i,\ell} := \oplus_{k=1}^4 V_{\ell,k}^i$. Then the number of basis functions in $V_{i,\ell}$ is $4 \times 2^\ell = 2^{\ell+2}$. Denote these basis functions as v_k for $k = 1, \cdots, 2^{\ell+2}$.
2.	Calculate local multiscale basis $\mathcal{L}_i^{-1}(v_k)$ for all $k = 1, \cdots, 2^{\ell+2}$. Here, $\mathcal{L}_i^{-1}(v_k) := v$ satisfies: $\begin{cases} \mathcal{L}_i v := -\nabla\cdot(\kappa\nabla v) = 0 & \text{in } \omega_i, \\ v = v_k & \text{on } \partial\omega_i. \end{cases}$
3.	Build global multiscale space. $V_{\text{ms},\ell}^{\text{EW}} := \text{span}\{\chi_i\mathcal{L}_i^{-1}(v_k), \chi_i v^i :\ 1 \leq i \leq N,\ \ 1 \leq k \leq 2^{\ell+2}\}$.
4.	Solve for (2.5) by conforming Galerkin method in $V_{\text{ms},\ell}^{\text{EW}}$ to obtain $u_{\text{ms},\ell}^{\text{EW}}$.

Algorithm 2 proceeds as follows. As in Algorithm 1, we first construct the local multiscale basis functions on each coarse neighborhood ω_i. Given a level parameter $\ell \in \mathbb{N}$, and the four coarse edges $\Gamma_{i,k}$ with $k = 1, 2, 3, 4$, i.e., $\cup_{k=1}^4 \Gamma_{i,k} = \partial\omega_i$, let $V_{\ell,k}^i$ be either the hierarchical bases or Haar wavelets up to level ℓ on the coarse edge $\Gamma_{i,k}$. Note that we will drop the superscript for the subspaces $V_{i,\ell}^{\text{I}}$ and $V_{i,\ell}^{\text{II}}$. Let $V_{i,\ell} := \oplus_{k=1}^4 V_{\ell,k}^i$ be the edge basis functions on $\partial\omega_i$. Then $V_{i,\ell}$ becomes a good approximation space of dimension $2^{\ell+2}$ to the trace of the solution over $\partial\omega_i$, i.e., $u|_{\partial\omega_i}$.

Subsequently, we calculate the κ-harmonic functions on each coarse neighborhood ω_i with all possible Dirichlet boundary conditions in $V_{i,\ell}$, and denote the resulting local multiscale space as $\mathcal{L}_i^{-1}(V_{i,\ell})$ in Step 2. Analogous to Algorithm 1, we can then define the global multiscale space as $V_{\text{ms},\ell}^{\text{EW}}$ and obtain the multiscale solution $u_{\text{ms},\ell}^{\text{EW}}$ in Steps 3 and 4.

Remark 4.2 *(WEMsFEM is an extension of MsFEM proposed in [11]).* Let $\ell := 0$, then the local multiscale basis functions $\mathcal{L}_i^{-1}(V_{i,0})$ generated in Step 2 of Algorithm 2 contain the constant basis function. Since the multiscale basis functions proposed in [11] serve as the partition of unity functions, cf. (4.1), Step 3 of Algorithm 2 implies that $\{\chi_i\}_{i=1}^N \subset V_{\mathrm{ms},0}^{\mathrm{EW}}$. Consequently, our proposed WEMsFEM is one enrichment of the classical multiscale method (MsFEM).

Remark 4.3. Let n be the number of fine elements in each coarse element, respectively. For the sake of simplicity, we can take $n := 2^m$ for some positive constant $m \in \mathbb{N}$. However, this is not mandatory since we can always use interpolation operator to connect the fine grids $\mathcal{T}_h$ with the mesh grids h_ℓ for Haar wavelets or hierarchical bases of level ℓ.

Remark 4.4 *(Flexibility of the Wavelet-based edge multiscale basis functions).* The Wavelet-based edge multiscale basis functions can be potentially extended to more general PDEs with heterogeneous coefficients since the only modification is to replace the local operator $\mathcal{L}_i$ in Algorithm 2 with the localized PDEs.

5. Error estimate

This section is concerned with deriving the convergence rates of Algorithm 1 and Algorithm 2 for elliptic problems with heterogeneous coefficients, cf. Problem (2.1).

We will first recap several results from [14]. The solution u satisfies the following equation

$$\begin{cases} -\nabla\cdot(\kappa\nabla u) = f & \text{in } \omega_i, \\ -\kappa\dfrac{\partial u}{\partial n} = -\kappa\dfrac{\partial u}{\partial n} & \text{on } \partial\omega_i, \end{cases}$$

which can be split into three parts, namely

$$u|_{\omega_i} = u^{i,\mathrm{I}} + u^{i,\mathrm{II}} + u^{i,\mathrm{III}}. \tag{5.1}$$

Here, the three components $u^{i,\mathrm{I}}$, $u^{i,\mathrm{II}}$, and $u^{i,\mathrm{III}}$ are respectively given by

$$\begin{cases} -\nabla\cdot(\kappa\nabla u^{i,\mathrm{I}}) = f - \bar{f}_i & \text{in } \omega_i \\ -\kappa\dfrac{\partial u^{i,\mathrm{I}}}{\partial n} = 0 & \text{on } \partial\omega_i, \end{cases} \tag{5.2}$$

where $\bar{f}_i := \int_{\omega_i} f\,\mathrm{d}x \times \frac{\widetilde{\kappa}}{\int_{\omega_i}\widetilde{\kappa}\,\mathrm{d}x}$,

$$\begin{cases} -\nabla\cdot(\kappa\nabla u^{i,\mathrm{II}}) = 0 & \text{in } \omega_i \\ -\kappa\dfrac{\partial u^{i,\mathrm{II}}}{\partial n} = -\kappa\dfrac{\partial u}{\partial n} - \fint_{\partial\omega_i}\kappa\dfrac{\partial u}{\partial n} & \text{on } \partial\omega_i, \end{cases}$$

and

$$u^{i,\mathrm{III}} = v^i \int_{\omega_i} f\,\mathrm{d}x$$

with v^i being defined in Algorithm 1. Clearly, $u^{i,\mathrm{III}}$ involves only one local solver.

The convergence of the edge spectral basis functions is a direct consequence of the results in [14]. One main observation in [14] is that the edge spectral basis functions play the critical role in the convergence analysis should the convergence rate of $\mathcal{O}(H)$ be after. Note that Algorithm 1 discards the first component $u^{i,\mathrm{I}}$ compared with [14], we only need to establish an a priori estimate for this term, which is presented in the following:

Lemma 5.1. *Let $f \in L^2(D)$, then there holds*

$$\begin{cases} \left\|u^{i,\mathrm{I}}\right\|_{H^1_\kappa(\omega_i)} \lesssim H\,\|f\|_{L^2(\omega_i)} \\ \left\|u^{i,\mathrm{I}}\right\|_{L^2_{\widetilde{\kappa}}(\omega_i)} \lesssim H^2\left\|\widetilde{\kappa}\right\|^{1/2}_{L^\infty(\omega_i)}\|f\|_{L^2(\omega_i)}. \end{cases} \tag{5.3}$$

Proof. Testing (5.2) with $u^{i,\mathrm{I}}$, and noting that $\kappa > 1$ and $\int_{\omega_i} f - \bar{f}_i\,\mathrm{d}x = 0$, yields the first estimate.

Next, we prove the second estimate. Indeed, since $\int_{\omega_i} \widetilde{\kappa} u^{i,\mathrm{I}} \,\mathrm{d}x = 0$, we arrive at

$$\left\| u^{i,\mathrm{I}} \right\|^2_{L^2_{\widetilde{\kappa}}(\omega_i)} = \int_{\omega_i} \widetilde{\kappa} u^{i,\mathrm{I}} (u^{i,\mathrm{I}} - \bar{u}^{i,\mathrm{I}}) \,\mathrm{d}x \leq \|\widetilde{\kappa}\|_{L^\infty(\omega_i)} \left\| u^{i,\mathrm{I}} - \bar{u}^{i,\mathrm{I}} \right\|^2_{L^2(\omega_i)}.$$

Here, $\bar{u}^{i,\mathrm{I}} := |\omega_i|^{-1} \int_{\omega_i} u^{i,\mathrm{I}} \,\mathrm{d}x$ is the average of $u^{i,\mathrm{I}}$ over the coarse neighborhood ω_i.

Finally, an application of the Poincaré's inequality together with the first estimate in (5.3) reveals the second assertion. This completes the proof. □

Proposition 5.1 *(Error estimate for Algorithm 1 to Problems (2.1)). Let Assumption 2.1 hold. Assume that $f \in L^2_{\widetilde{\kappa}^{-1}}(D) \cap L^2(D)$ and let $\ell_i \in \mathbb{N}_+$ for all $i = 1, 2, \cdots, N$. Let $u \in V$ be the solutions to Problems (2.1). There holds*

$$\begin{aligned} |u - u^{\mathrm{ES}}_{\mathrm{ms}}|_{H^1_\kappa(D)} &:= \min_{w \in V^{\mathrm{ES}}_{\mathrm{ms}}} |u - w|_{H^1_\kappa(D)} \\ &\lesssim H \|\widetilde{\kappa}\|^{1/2}_{L^\infty(D)} \|f\|_{L^2_{\widetilde{\kappa}^{-1}}(D)} + \max_{i=1,\cdots,N} \left\{ (H\lambda^{\mathrm{T}_i}_{\ell_i})^{-\frac{1}{2}} \right\} \|f\|_{L^2(D)}. \end{aligned} \tag{5.4}$$

Proof. This result follows from Proposition 4.1 and Remark 4.2 in [14]. □

As mentioned earlier, we will focus only on the Haar wavelets in Algorithm 2 since the convergence of Algorithm 2 using Hierarchical bases can be obtained in a similar manner. In the following, we define the $L^2(\partial\omega_i)$-orthogonal projection $\mathcal{P}_{i,\ell}$ onto the local multiscale space up to level ℓ: $L^2(\partial\omega_i) \to V_{i,\ell}$ by

$$\mathcal{P}_{i,\ell}(v) := \sum_{j=1}^{2^{\ell+2}} (v, \psi_j)_{\partial\omega_i} \mathcal{L}_i^{-1}(\psi_j) \quad \text{for all } v \in L^2(\partial\omega_i). \tag{5.5}$$

Here, we denote ψ_j for $j = 1, \cdots 2^{\ell+2}$ as the Haar wavelets defined on the four edges of ω_i of level ℓ and the local operator $\mathcal{L}_i$ is defined as in Algorithm 2.

To prove the convergence of the wavelet-based edge multiscale basis functions in Subsection 4.2, we will first approximate the second component $u^{i,\mathrm{II}}$ by the wavelet-based edge multiscale basis functions. On the one hand, notice that $u^{i,\mathrm{II}} \in H^{1/2}(\partial\omega_i)$, then we can obtain by Proposition 3.1 combining with a scaling argument, that

$$\|u^{i,\mathrm{II}} - \mathcal{P}_{i,\ell} u^{i,\mathrm{II}}\|_{L^2(\partial\omega_i)} \lesssim \sqrt{H} 2^{-\ell/2} |u^{i,\mathrm{II}}|_{H^{1/2}(\partial\omega_i)}.$$

Here, $|\cdot|_{H^{1/2}(\partial\omega_i)}$ denotes the Gargliardo (semi) norm for the fractional Sobolev space $H^{1/2}(\partial\omega_i)$.

On the other hand, since $\kappa \geq 1$, then an application of the Trace inequality leads to

$$|u^{i,\mathrm{II}}|_{H^{1/2}(\partial\omega_i)} \lesssim |u^{i,\mathrm{II}}|_{H^1(\omega_i)} \lesssim |u^{i,\mathrm{II}}|_{H^1_\kappa(\omega_i)}.$$

Plugging this estimate into the previous one results in

$$\|u^{i,\mathrm{II}} - \mathcal{P}_{i,\ell} u^{i,\mathrm{II}}\|_{L^2(\partial\omega_i)} \lesssim \sqrt{H} 2^{-\ell/2} |u^{i,\mathrm{II}}|_{H^1_\kappa(\omega_i)}. \tag{5.6}$$

Now we are ready to present the estimate for the second algorithm:

Proposition 5.2 *(Error estimate for Algorithm 2 to Problems (2.1)). Let Assumption 2.1 hold. Assume that $f \in L^2_{\widetilde{\kappa}^{-1}}(D) \cap L^2(D)$ and let $\ell \in \mathbb{N}_+$. Let $u \in V$ be the solutions to Problems (2.1). There holds*

$$\begin{aligned} |u - u^{\mathrm{EW}}_{\mathrm{ms},\ell}|_{H^1_\kappa(D)} &:= \min_{w \in V^{\mathrm{EW}}_{\mathrm{ms}}} |u - w|_{H^1_\kappa(D)} \\ &\lesssim H \|\widetilde{\kappa}\|^{1/2}_{L^\infty(D)} \|f\|_{L^2_{\widetilde{\kappa}^{-1}}(D)} + 2^{-\ell/2} \|\kappa\|_{L^\infty(\mathcal{F}_H)} \|f\|_{L^2(D)}. \end{aligned} \tag{5.7}$$

Proof. On the one hand, [14, Lemma 4.1] shows

$$|u^{i,\mathrm{II}}|_{H^1_\kappa(\omega_i)} \lesssim |u|_{H^1_\kappa(\omega_i)} + H\|f\|_{L^2(\omega_i)}. \tag{5.8}$$

Then the trace approximation (5.6) and similar proof to [14, Lemma 4.4] lead to

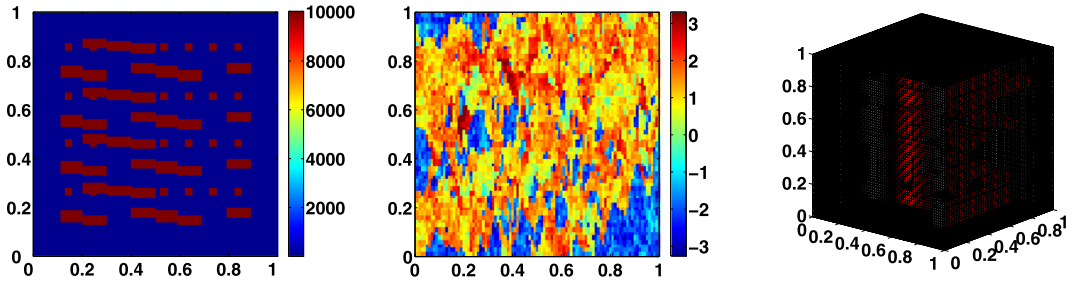

(a) Model 1 (b) Model 2 ($\log_{10}$ scale) (c) Model 3

Fig. 2. Permeability fields κ. (For interpretation of the colors in the figure(s), the reader is referred to the web version of this article.)

$$\|u^{i,\mathrm{II}} - \mathcal{P}_{i,\ell}u^{i,\mathrm{II}}\|_{L^2_\kappa(\partial\omega_i)} \lesssim \sqrt{H}2^{-\ell/2}\|\kappa\|^{1/2}_{L^\infty(\partial\omega_i)}\Big(|u|_{H^1_\kappa(\omega_i)} + H\|f\|_{L^2_{\kappa^{-1}}(\omega_i)}\Big), \tag{5.9}$$

$$\Big\|u^{i,\mathrm{II}} - \mathcal{P}_{i,\ell}u^{i,\mathrm{II}}\Big\|_{L^2_{\widetilde{\kappa}}(\omega_i)} \lesssim H2^{-\ell/2}\|\kappa\|^{1/2}_{L^\infty(\partial\omega_i)}\Big(|u|_{H^1_\kappa(\omega_i)} + H\|f\|_{L^2_{\kappa^{-1}}(\omega_i)}\Big), \tag{5.10}$$

$$\int_{\omega_i}\chi_i^2\kappa|\nabla(u^{i,\mathrm{II}} - \mathcal{P}_{i,\ell}u^{i,\mathrm{II}})|^2\,\mathrm{d}x \lesssim 2^{-\ell}H^{-1}\|\kappa\|_{L^\infty(\partial\omega_i)}\Big(|u|^2_{H^1_\kappa(\omega_i)} + H^2\|f\|^2_{L^2_{\kappa^{-1}}(\omega_i)}\Big). \tag{5.11}$$

Now we prove the energy error estimate. Let

$$\widetilde{u}_i := \mathcal{P}_{i,\ell}u^{i,\mathrm{II}} + u^{i,\mathrm{III}}. \tag{5.12}$$

Denote $V^{\mathrm{EW}}_{\mathrm{ms},\ell} \ni w^{\mathrm{EW}}_{\mathrm{ms},\ell} := \sum_{i=1}^N \chi_i\widetilde{u}_i$ and $e := u - w^{\mathrm{S}}_{\mathrm{off}}$. Then similar proof as in [14, Lemma 4.5] leads to

$$\begin{aligned}\int_D \kappa|\nabla e|^2\,\mathrm{d}x \lesssim &\sum_{i=1}^N\Big(H^{-2}\int_{\omega_i}\widetilde{\kappa}|u^{i,\mathrm{I}}|^2\,\mathrm{d}x + \int_{\omega_i}\kappa|\nabla u^{i,\mathrm{I}}|^2\,\mathrm{d}x\Big)\\ &+\sum_{i=1}^N\Big(H^{-2}\int_{\omega_i}\widetilde{\kappa}|u^{i,\mathrm{II}} - \mathcal{P}_{i,\ell}u^{i,\mathrm{II}}|^2\,\mathrm{d}x + \int_{\omega_i}\chi_i^2\kappa|\nabla(u^{i,\mathrm{II}} - \mathcal{P}_{i,\ell}u^{i,\mathrm{II}})|^2\,\mathrm{d}x\Big).\end{aligned}$$

This, together with the error estimates (5.9)-(5.11) and (5.3), and the Galerkin orthogonality property, proves the assertion. □

Notice that the energy error estimate in Proposition 5.2 depends on $\|\widetilde{\kappa}\|^{1/2}_{L^\infty(D)}$ and $\|\kappa\|_{L^\infty(\mathcal{F}_H)}$. This implies that if there is no high-contrast inclusion crosses the coarse edges $\mathcal{F}_H$, then this estimate will be independent of the high-contrast parameter κ. Consequently, we only need to choose the level parameter $\ell := \lceil -\log_2 H\rceil$. In the general situation when some high-contrast inclusions crosse the coarse edges $\mathcal{F}_H$, it is not yet known the dependence of $\|\widetilde{\kappa}\|^{1/2}_{L^\infty(D)}$ on the high-contrast parameter κ. This requires further investigation.

Remark 5.1. Under the assumption that $\|\widetilde{\kappa}\|^{1/2}_{L^\infty(D)}$ is bounded, we can infer from Proposition 5.2 that the energy error can be bounded above by $\mathcal{O}(H)$, should the number of level $\ell := \lceil -\log_2 H\rceil + \lceil \log_2\|\kappa\|_{L^\infty(\mathcal{F}_H)}\rceil$ become. Nevertheless, one can observe from the numerical tests that this algorithm actually is much more accurate than we have proved. This is mainly due to the fact that we employed the lowest regularity on each coarse edge and the worst scenario that high-contrast regions cross the coarse grid $\mathcal{T}_H$, namely, $u|_{\partial\omega_i} \in H^{1/2}(\partial\omega_i)$, in the convergence analysis, cf. (5.6).

6. Numerical tests

In this section, we present several numerical tests to demonstrate the accuracy of our proposed methods. In specific, we apply the multiscale algorithms ESMsFEM and WEMsFEM to solve the heterogeneous elliptic problem (2.1).

In our experiments, we take the computational domain $D := [0,1]^d$, for $d = 2$ and 3 and the constant force is employed, namely $f := 1$. Let $\mathcal{T}_H$ be a regular quasi-uniform rectangular mesh over D with maximal mesh size H and let $\mathcal{T}_h$ be a regular quasi-uniform rectangular mesh over each coarse element $T \in \mathcal{T}_H$ with maximal mesh size h. Let $h := \sqrt{2}\times 2^{-9}$ for $d = 2$, and $h := \sqrt{2}\times 2^{-6}$ for $d = 3$.

We test our methods for the heterogeneous elliptic problem with the permeability fields κ as depicted in Fig. 2. Note that the fine scale h can resolve these permeability fields. In specific, the second permeability field is the projection of the 85th layer of the tenth SPE comparative solution project (SPE 10), cf. [1], onto the fine mesh $\mathcal{T}_h$. In this manner, the fine

Table 1
Convergence history of WEMsFEM based on Haar wavelets for Problem (2.1) with Model 1.

H	$\ell=0$		$\ell=1$		$\ell=2$	
	e_{L^2}	e_{H^1}	e_{L^2}	e_{H^1}	e_{L^2}	e_{H^1}
$\sqrt{2}/8$	13.81 %	28.37%	3.52 %	14.18%	0.31 %	4.11%
$\sqrt{2}/16$	6.44%	19.07%	0.26 %	4.74%	0.05%	2.43%
$\sqrt{2}/32$	2.31%	13.15%	0.17%	3.80%	0.03%	1.79%
$\sqrt{2}/64$	0.86%	8.16%	0.08%	2.61%	0.01%	0.95%

Table 2
Convergence history of WEMsFEM based on hierarchical bases for Problem (2.1) with Model 1.

H	$\ell=0$		$\ell=1$		$\ell=2$	
	e_{L^2}	e_{H^1}	e_{L^2}	e_{H^1}	e_{L^2}	e_{H^1}
$\sqrt{2}/8$	7.84%	22.96%	2.58%	11.94%	0.20%	3.59%
$\sqrt{2}/16$	6.39%	19.72%	0.73%	6.62%	0.03%	1.82%
$\sqrt{2}/32$	5.03%	17.02%	0.22%	4.05%	0.01%	0.85%
$\sqrt{2}/64$	1.50%	10.40%	0.05%	1.89%	0.0024%	0.42%

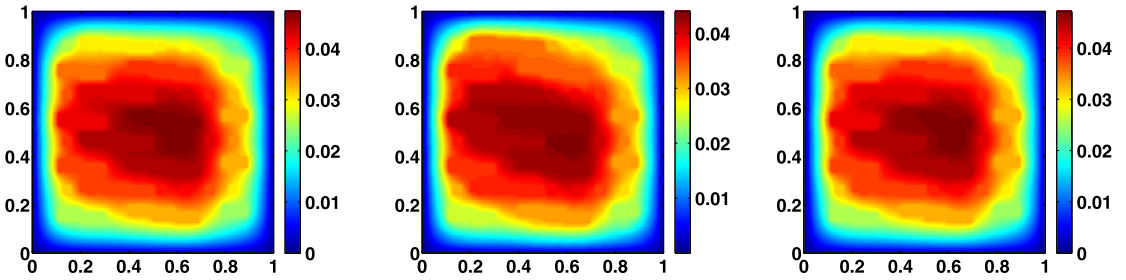

(a) Reference solution (b) WEMsFEM solution, $\ell = 0$ (c) WEMsFEM solution, $\ell = 1$

Fig. 3. The reference solution and the multiscale solutions with $H = \sqrt{2}/16$, obtained from WEMsFEM based on Haar wavelets with levels $\ell = 0$ and 1 for Problem (2.1) with Model 1.

mesh $\mathcal{T}_h$ can fit the microscale features in Model 2. In Model 3, we take $\kappa := 1$ in the background $\kappa := 10^4$ in the red region.

In addition, to quantify the accuracy of the multiscale solutions obtained from our proposed methods, namely, ESMsFEM and WEMsFEM, we define relative weighted L^2 error and energy error as follows:

$$e_{L^2} = \frac{||\kappa^{1/2}(u_{ms} - u_h)||_{L^2(D)}}{||\kappa^{1/2}u_h||_{L^2(D)}}, \quad e_{H^1} = \sqrt{\frac{a(u_{ms} - u_h, u_{ms} - u_h)}{a(u_h, u_h)}}.$$

Recall that u_h is the fine-scale solution in the finite element space V_h derived from conforming Galerkin scheme, cf. (2.3).

6.1. Numerical tests for WEMsFEM

Tables 1 and 2 show the numerical results of WEMsFEM with Haar and hierarchical bases for the test model 1. We range the coarse mesh size H from $\sqrt{2}/8$ to $\sqrt{2}/64$, and the wavelet level ℓ from 0 to 2. One can observe that the accuracy of the WEMsFEM solution can be improved as the coarse mesh size H is decreasing and wavelet level ℓ is enlarging. When the wavelet level $\ell = 0$, we observe that WEMsFEM based on the Haar wavelets outperforms that based on the hierarchical bases, while the opposite scenario occurs in the case when $\ell = 1, 2$. Let N_{dof} be the total number of multiscale basis functions, then one can compute the convergence rate of WEMsFEM with respect to the parameter N_{dof}. Tables 1 and 2 shows that the convergence rate exceeds $\mathcal{O}(N_{\text{dof}}^{-1})$. This result is much better than our expectation, i.e., $\mathcal{O}(N_{\text{dof}}^{-1/2})$ with much smaller parameter ℓ.

We depict in Fig. 3 the reference solution, the multiscale solutions solved by WEMsFEM based on Haar wavelets with the level $\ell = 0$ and 1 for Problem (2.1) with Model 1. When $\ell = 0$, the multiscale solution fails to capture the microscale features introduced by the complicated heterogeneity in Model 1. Nevertheless, the multiscale solution with wavelet level $\ell = 1$ is sufficient to generate a good approximation to the reference solution.

Furthermore, we present in Tables 3 and 4 the convergence history of WEMsFEM for Problem (2.1) with Model 2 based on Haar wavelets and hierarchical bases, respectively. Similar convergence behavior as in Tables 1 and 2 for Model 1 can be observed. One can obtain a slower convergence rate of $\mathcal{O}(N_{\text{dof}}^{-1/2})$ compared to Model 1, which arises from the more

Table 3
Convergence history of WEMsFEM based on Haar wavelets for Problem (2.1) with Model 2.

H	$\ell=0$		$\ell=1$		$\ell=2$	
	e_{L^2}	e_{H^1}	e_{L^2}	e_{H^1}	e_{L^2}	e_{H^1}
$\sqrt{2}/8$	3.82%	41.98%	2.19%	34.46%	1.17%	25.17%
$\sqrt{2}/16$	2.70%	36.24%	1.01%	25.51%	0.41%	16.88%
$\sqrt{2}/32$	1.32%	24.11%	0.33%	14.81%	0.13%	10.17%
$\sqrt{2}/64$	0.85%	16.95%	0.14%	8.81%	0.04%	5.75%

Table 4
Convergence history of WEMsFEM based on hierarchical bases for Problem (2.1) with Model 2.

H	$\ell=0$		$\ell=1$		$\ell=2$	
	e_{L^2}	e_{H^1}	e_{L^2}	e_{H^1}	e_{L^2}	e_{H^1}
$\sqrt{2}/8$	4.18%	48.78%	1.86 %	33.20%	1.11%	25.04%
$\sqrt{2}/16$	2.65%	41.20%	1.03%	26.44%	0.37 %	16.88%
$\sqrt{2}/32$	1.59%	30.50%	0.28%	19.50%	0.12%	10.09%
$\sqrt{2}/64$	0.82%	20.54%	0.10%	9.29%	0.04 %	5.59%

Table 5
Convergence history of WEMsFEM based on hierarchical bases and hierarchical bases with level of $\ell=0$ for Problem (2.1) with Model 3.

H	Haar wavelets		hierarchical bases	
	e_{L^2}	e_{H^1}	e_{L^2}	e_{H^1}
$\sqrt{2}/8$	6.85%	20.41%	9.52%	28.5%
$\sqrt{2}/16$	9.04%	21.50%	9.45%	22.4%

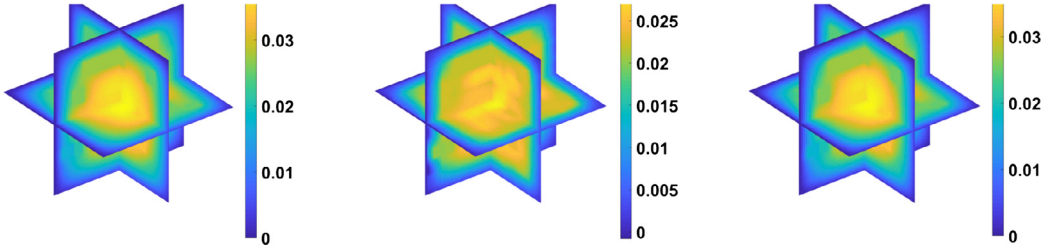

(a) Reference solution (b) ESMsFEM solution: $N_b = 2$. (c) ESMsFEM solution: $N_b = 8$.

Fig. 4. The reference solution and the ESMsFEM solutions with $N_b = 2$ and 8 for Model 3 and $H = \sqrt{2}/8$.

heterogeneous features in Model 2. Due to limited computational resources, we only test the WEMsFEM for Model 3 with wavelets level of $\ell = 0$. Its convergence history is depicted in Table 5. As expected, the resulted multiscale solutions are not sufficiently accurate.

6.2. Numerical tests for ESMsFEM

In these numerical tests, we take the same number of local multiscale spectral basis functions $N_b \in \mathbb{N}_+$ for each coarse neighborhood ω_i, where $i \in \{1, \cdots, N\}$ denotes the coarse grid index. Recall that $N \in \mathbb{N}_+$ is the total number of coarse grids in the coarse mesh $\mathcal{T}_H$. Let Λ be the minimum of the eigenvalues corresponding to the first eigenfunction defined in Algorithm 1, which are not included in the multiscale space $V_{\text{off}}^{\text{ES}}$:

$$\Lambda = \min_{i=1,\cdots,N} \left\{ \lambda_{N_b+1}^{\mathrm{T}_i} \right\}.$$

We depict the reference solution and the multiscale solutions obtained from the ESMsFEM scheme with $H = \sqrt{2}/8$ and $N_b = 2$ and 8 for Model 3 in Fig. 4. One can conclude that the multiscale solution from ESMsFEM with $N_b = 8$ is sufficient to characterize the microscale features hidden in Model 3.

The convergence history of the edge spectral multiscale method (ESMsFEM) for Problem (2.1) with Models 1, 2 and 3 are presented in Tables 6-11. As proved in Proposition 5.1, the multiscale solution solved by ESMsFEM converges as Λ increases and the coarse mesh size H decreases. We take Model 1 for an instance. Let $H := \sqrt{2}/32$, then the L^2 relative error decays

Table 6
Convergence history of ESMsFEM for Problem (2.1) with Model 1 and $H = \sqrt{2}/32$.

N_b	Λ	e_{L^2}	e_{H^1}
2	74.7	3.82%	16.36%
4	186.4	0.37%	5.95%
6	347.6	0.21%	4.53%
8	529.4	0.05%	2.25%
10	743.2	0.02%	1.43%

Table 7
Convergence history of ESMsFEM for Problem (2.1) with Model 1 and $H = \sqrt{2}/64$.

N_b	Λ	e_{L^2}	e_{H^1}
2	440783.8	1.13%	9.26%
4	640000.0	0.13%	3.36%
6	1496214.7	0.08%	2.74%
8	1537887.8	0.01%	0.95%
10	2556030.5	0.003%	0.50%

Table 8
Convergence history of ESMsFEM for Problem (2.1) with Model 2 and $H = \sqrt{2}/32$.

N_b	Λ	e_{L^2}	e_{H^1}
2	1558.2	16.33%	35.72%
4	3760.2	10.29%	26.85%
6	5493.2	8.58%	24.16%
8	8195.6	7.33%	22.45%
10	9772.0	6.60%	21.23%

Table 9
Convergence history of ESMsFEM for Problem (2.1) with Model 2 and $H = \sqrt{2}/64$.

N_b	Λ	e_{L^2}	e_{H^1}
2	47812.7	7.91%	26.97%
4	86609.2	4.02%	18.00%
6	116963.8	2.77%	14.58%
8	187984.5	2.08%	12.71%
10	212675.7	1.63%	11.46%

Table 10
Convergence history of ESMsFEM for Problem (2.1) with Model 3 and $H = \sqrt{2}/8$.

N_b	Λ	e_{L^2}	e_{H^1}
2	8.4	17.87%	38.92%
4	12.6	7.58%	23.5%
6	15.3	1.73%	10.6%
8	17.9	0.96%	7.83%
10	27.0	0.71%	6.20%

from 3.82% to 0.02% as the number of bases N_b increases from 2 to 10. As expected, ESMsFEM works better for model 1 compared with model 2 due to the high heterogeneity in model 2, see Tables 6, 7, 8 and 9.

We present the numerical tests for Model 3 in Tables 10 and 11 corresponding to different coarse mesh sizes of $H = \sqrt{2}/8$ and $H = \sqrt{2}/16$. Due to limited computational resources, the case for much finer coarse grid is not performed. Compared with the numerical results for WEMsFEM, cf. Table 5, ESMsFEM performs much better in this case. Nevertheless, ESMsFEM involves solving local eigenvalue problems and thus has much higher computational cost than WEMsFEM.

Finally, to emphasize the accuracy of the proposed methods, we provide the performance of the (oversampling) Multiscale Finite Element Methods (MsFEMs) in Tables 12, 13 and 14 for the three tested permeability fields Models 1 to 3, respectively. Here, we denote K^+ as the oversampled region. In the case that $K^+ = K$, there is no oversampling and the local multiscale basis functions are solved on each coarse element K, cf. (4.1); when $K^+ = K + \frac{\eta}{2}$, the local multiscale func-

Table 11
Convergence history of ESMsFEM for Problem (2.1) with Model 3 and $H = \sqrt{2}/16$.

N_b	Λ	e_{L^2}	e_{H^1}
2	28.1	13.9%	26.3%
4	40.6	1.95%	11.7%
6	56.7	0.33%	4.80%
8	60.8	0.12%	3.30%
10	76.7	0.06%	2.30%

Table 12
Convergence history of (oversampling) MsFEM for Problem (2.1) with Model 1.

H	$K^+ = K$		$K^+ = K + \frac{n}{2}$		$K^+ = K + n$	
	e_{L^2}	e_{H^1}	e_{L^2}	e_{H^1}	e_{L^2}	e_{H^1}
$\sqrt{2}/8$	96.96%	98.29%	3.92%	3235.69%	3.81%	3373.30%
$\sqrt{2}/16$	35.97%	53.02%	19.70%	619.32%	0.74%	434.93%
$\sqrt{2}/32$	18.59%	36.64%	16.45%	90.00%	9.29%	82.95%
$\sqrt{2}/64$	6.24%	21.22%	5.09%	266.35%	3.69%	242.37%

Table 13
Convergence history of (oversampling) MsFEM for Problem (2.1) with Model 2.

H	$K^+ = K$		$K^+ = K + \frac{n}{2}$		$K^+ = K + n$	
	e_{L^2}	e_{H^1}	e_{L^2}	e_{H^1}	e_{L^2}	e_{H^1}
$\sqrt{2}/8$	41.12%	88.20%	13.59%	171.20%	12.62%	263.41%
$\sqrt{2}/16$	38.97%	72.05%	9.56%	523.75%	13.84%	718.14%
$\sqrt{2}/32$	29.54%	61.24%	7.87%	436.88%	7.24%	379.40%
$\sqrt{2}/64$	16.70%	50.51%	3.14%	234.27%	2.70%	179.93%

Table 14
Convergence history of (oversampling) MsFEM for Problem (2.1) with Model 3.

H	$K^+ = K$		$K^+ = K + \frac{n}{2}$		$K^+ = K + n$	
	e_{L^2}	e_{H^1}	e_{L^2}	e_{H^1}	e_{L^2}	e_{H^1}
$\sqrt{2}/8$	95.21%	97.16%	58.94%	11.33%	12.62%	410.29%
$\sqrt{2}/16$	26.42%	42.76%	21.41%	306.23%	10.89%	162.74%

tions are solved in a larger domain with an extra half coarse element in each direction; when $K^+ = K + n$, then the local multiscale basis functions are solved in a much larger domain with one extra coarse element in each direction.

According to the numerical results, we notice that the numerical solutions solved by (oversampling) MsFEMs result in a relatively decent approximation to the reference solution measured by weighted L^2 norm. However, they are far from satisfactory should they be measured in the energy norm. One observes that the utilization of oversampling technique is detrimental to the approximation in energy norm. One possible explanation lies in the nonconforming nature of the multiscale basis functions when the oversampling technique is employed.

7. Conclusions

We proposed in this paper two new types of edge multiscale method in the framework of the Generalized Multiscale Finite Element Methods (GMsFEMs), with their local multiscale basis functions being defined on each coarse edge. Their theoretical convergence rates were elaborately justified in terms of the number of local multiscale basis functions, the level of the wavelets and the coarse scale mesh size. Especially, the constants appearing in the estimates are independent of the multiple scales and large deviation of values in the heterogeneous coefficients. To verify our theoretical results, extensive numerical performance for elliptic problems with high-contrast heterogeneous coefficients are demonstrated. Our new proposed algorithms opens up a new direction for multiscale methods both theoretically and numerically. Future applications include convection dominated diffusion problems and Helmholtz equations with high frequencies.

References

[1] J. Aarnes, V. Kippe, K.-A. Lie, Mixed multiscale finite elements and streamline methods for reservoir simulation of large geomodels, Adv. Water Resour. 28 (2005) 257–271.
[2] L. Berlyand, H. Owhadi, Flux norm approach to finite dimensional homogenization approximations with non-separated scales and high contrast, Arch. Ration. Mech. Anal. 198 (2) (2010) 677–721.

[3] C.-C. Chu, I. Graham, T. Hou, A new multiscale finite element method for high-contrast elliptic interface problems, Math. Compet. 79 (272) (2010) 1915–1955.
[4] I. Daubechies, Ten Lectures on Wavelets, CBMS-NSF Regional Conference Series in Applied Mathematics, vol. 61, Society for Industrial and Applied Mathematics (SIAM), Philadelphia, PA, 1992.
[5] W. E, B. Engquist, The heterogeneous multiscale methods, Commun. Math. Sci. 1 (1) (2003) 87–132.
[6] Y. Efendiev, J. Galvis, T. Hou, Generalized multiscale finite element methods, J. Comput. Phys. 251 (2013) 116–135.
[7] Y. Efendiev, J. Galvis, X.-H. Wu, Multiscale finite element methods for high-contrast problems using local spectral basis functions, J. Comput. Phys. 230 (4) (2011) 937–955.
[8] B. Engquist, O. Runborg, Wavelet-based numerical homogenization with applications, in: Multiscale and Multiresolution Methods, Springer, 2002, pp. 97–148.
[9] M. Griebel, M. Schweitzer, A particle-partition of unity method for the solution of elliptic, parabolic and hyperbolic PDE, SIAM J. Sci. Comput. 22 (3) (2000) 853–890.
[10] T. Hou, P. Liu, Optimal local multi-scale basis functions for linear elliptic equations with rough coefficient, Discrete Contin. Dyn. Syst. 36 (8) (2016) 4451–4476.
[11] T. Hou, X.-H. Wu, A multiscale finite element method for elliptic problems in composite materials and porous media, J. Comput. Phys. 134 (1) (1997) 169–189.
[12] T. Hughes, G. Feijóo, L. Mazzei, J.-B. Quincy, The variational multiscale method—a paradigm for computational mechanics, Comput. Methods Appl. Mech. Eng. 166 (1–2) (1998) 3–24.
[13] G. Li, Low-rank approximation to heterogeneous elliptic problems, Multiscale Model. Simul. 16 (1) (2018) 477–502.
[14] G. Li, On the convergence rates of GMsFEMs for heterogeneous elliptic problems without oversampling techniques, Multiscale Model. Simul. 17 (2) (2019) 593–619.
[15] G. Li, D. Peterseim, M. Schedensack, Error analysis of a variational multiscale stabilization for convection-dominated diffusion equations in two dimensions, IMA J. Numer. Anal. 38 (3) (2018) 1229–1253.
[16] J.-L. Lions, E. Magenes, Non-Homogeneous Boundary Value Problems and Applications, vol. I, Springer-Verlag, New York-Heidelberg, 1972.
[17] A. Målqvist, D. Peterseim, Localization of elliptic multiscale problems, Math. Compet. 83 (290) (2014) 2583–2603.
[18] J. Melenk, I. Babuška, The partition of unity finite element method: basic theory and applications, Comput. Methods Appl. Mech. Eng. 139 (1–4) (1996) 289–314.
[19] H. Owhadi, Bayesian numerical homogenization, Multiscale Model. Simul. 13 (3) (2015) 812–828.
[20] H. Yserentant, On the multi-level splitting of finite element spaces, Numer. Math. 49 (4) (Jul 1986) 379–412.